

Bianchi type-V Transitioning model in Brans-Dicke theory with Observational Constraint

Vinod Kumar Bhardwaj¹, Archana Dixit², Anirudh Pradhan³

^{1,2}Department of Mathematics, Institute of Applied Sciences and Humanities, GLA University, Mathura-281 406, Uttar Pradesh, India

³Centre for Cosmology, Astrophysics and Space Science (CCASS), GLA University, Mathura-281 406, Uttar Pradesh, India

¹E-mail:dr.vinodbhardwaj@gmail.com

²E-mail:archana.dixit@gla.ac.in

³E-mail:pradhan.anirudh@gmail.com

Abstract

In this paper, we have examined the viability of the Bianchi type-V universe in Brans-Dicke (BD) theory of gravitation. We have discussed the interacting and non-interacting scenarios between dark matter (DM) and dark energy (DE) of the derived universe within the framework of BD theory. CCA technique has been applied to constrain the model parameters using 46 values of observational Hubble data (OHD), Pantheon data (the latest compilation of SNIa with 40 binned in the redshift range $0.014 \leq z \leq 1.62$) and their combined datasets. We establish an exact solution of the field equations to derive the dynamics of the derived universe and the obtained results are found to agree with the observations. We also noted a distinctive change in the sign of the deceleration parameter from positive to negative, as well as the presence of a transition red-shift exists. Using various observational data points, the evolution trajectories for $(r - s)$ diagnostic planes are shown to understand the geometrical behavior of the Bianchi-V model. Some physical properties of the universe are also discussed. It's also worth noting that the conclusions of the cosmological parameter are consistent with modern observational data.

Keywords : LRS Bianchi-V, Brans-Dicke theory, Λ CDM Model, Statefinders.

PACS: 98.80.-k

1 Introduction

According to recent studies of type Ia supernovae [1,2] our current universe is undergoing an accelerated phase of expansion preceded by a period of deceleration. To examine the current phase of acceleration, a new form of substance with negative pressure, called dark energy, has been suggested. In literature several models have been examined, to predict cosmic acceleration by assuming dark energy with repulsive gravity as the major content of the cosmos. According to the Planck observations, Universe's total mass-energy budget is composed of 68.3 % DE, 26.8 % dark matter and 4.9 % ordinary matter. This exotic form of energy is known as dark energy which is to be less effective in early times but dominates at the present epoch. The attracting

force of DM is involved in the creation of structure and clustering of galaxies.

Although several observational experiments support DE as a general clarification for the expansion mystery, but there are many questions which remain unanswered. The cosmological constant (Λ) has a repulsive nature, it is a usual candidate for DE. It possesses a low magnitude in comparison with prediction of particle physics. Apart from dark energy models, a variety of gravity theories such as $f(R)$ gravity [3, 4], $f(T)$ gravity [5], and $f(G)$ gravity [6, 7], $f(Q)$ gravity [?, 8], $f(Q, T)$ [10], Einstein-Gauss-Bonnet theory [11–15] were discussed. In the same direction, $f(R, T)$ theory is the another perspective of modified version of theory of gravity, which has been proposed by Harko et al. [16]. Similarly, many theories such as “scalar-tensor theories, scalar field theories, bimetric theories and vector-tensor theories [17, 18], Weyl theory [19], Lyra theory [20] Ylmaz theory [21] and Brans-Dicke theory [22, 23]” are some examples of these alternative gravitation theories [24]. For the previous coupled of decades, cosmologists have been interested in alternative theories of gravity, particularly “scalar-tensor” theories. Among all these alternative theories, the “Brans-Dicke theory (BDT)” is the one of the most successful alternate theory. Alonso et al. [25] have shown that the scalar tensor theory of Brans-Dicke type provides a relativistic generalization of Newtonian gravity in 2+1 dimensions. The theory is metric and test particles follow the space-time geodesics.

BD theory, on the other hand, is often considered as the prototype of a wide category of gravitational theories known as scalar-tensor theories. These theories are derived through a non-minimal coupling between the curvature scalar and a scalar field. These hypotheses have gotten a lot of interest in the cosmology community because they can accurately represent the early expansion of the universe [26]. The BD hypothesis predicts an extended period of inflation to address the universe’s graceful exit dilemma, as outlined by Mathiazhagan and Johri [27], La and Steinhardt [28]. Furthermore, with suitable parameter values, the theory can successfully construct late-time accelerated expansion without the contribution of DE ([29]) Several authors have been explored BD cosmology in different prospectives. The work of Singh and Rai [30] provides a detailed discussion of Brans-Dick cosmological models. Remarkable studies of BD theory with the application of a non-vanishing cosmological constant can be seen in [31–37]. In BD theory, authors [38–40] studied a model of accelerating universe with changeable deceleration parameter. In 1984 Brans-Dike cosmological model was investigated by taking Λ . The same idea was further extended inhomogeneous and anisotropic Bianchi type I spacetime [41, 42]. Akarsu, et al. [43] studied the anisotropic Λ CDM model with Brans-Dicke gravity. Recently, exact solutions of accelerating cosmological models in modified Brans-Dicke theory are proposed [44, 45].

In cosmology, Bianchi-type space-times play a very important role in comprehending and describing the early phases of the universe’s evolution. The study of Bianchi types II, VIII, and IX universe is particularly relevant since they correlate to well-known solutions such as the FRW universe with positive curvature, the de Sitter universe, the Taub-NUT solutions, and so on. The Bianchi type-V frame of reference is very important for developing the models for measuring the expansion of the Universe in its early stages [46, 47]. Several authors [48–53] have been interested in “Bianchi type-V space-time type over the last decade. The dynamical behavior of the Bianchi-V model is significantly more general than the simple FLRW model. The study of Bianchi type-V cosmological models creates more interest as these models contain isotropic special cases and permit arbitrarily small anisotropic levels at certain stages [54]. However, we know that, in recent years, Bianchi cosmological models have become extremely

important in observational cosmology, as evidenced by the WMAP observational data. It has validated an addition to the standard “ Λ CDM” model that resembles the Bianchi morphology. The WMAP data analysis supports the fact that the universe has a preferred direction and it should reach a slightly anisotropic geometry. Therefore, in view of the background anisotropy, the models with anisotropic backgrounds are more suitable to describe early stages of the universe [55, 56].

Cosmology is now one of the fastest-developing branches of science, particularly in terms of observations. In the last decade, cosmological data from various sources has been rapidly updated, not only in terms of quantity but also in terms of quality [57]. The latest “CMB anisotropies” results by “Planck Collaboration” provide the precise observations on temperature and polarization of the photons from the last scattering surface near the redshift about $z = 1090$ [58]. Another observable, which is worthy of mentioning, is the “redshift-space distortion (RSD)”. It has been measured more and more precisely in the past few years. This observable is a key signature to disclose the large-scale structure. In the present study, we proposed transitioning model of the universe Bianchi-V space-time in the framework of BD theory. To achieve the explicit solution for the model, we assumed the scalar field $\phi = \phi_0(t)[(e^{n\beta t} - 1)^{1/n}]^\eta$; where ϕ_0 , n , β and η are constants. In the present study, the recent OHD and Pantheon data sets are used to decide the model parameters “ n and β ” [59]. We investigate a transitioning model of the universe for interacting and non-interacting scenarios within the framework of Brans-Dicke theory.

In our derived model, the best fit values of parameters are determined by using χ^2 statistic. Two observational data sets, i) A data set of 46 OHD and ii) Pantheon data (the latest compilation of SNIa with 40 binned in the redshift range $0.014 \leq z \leq 1.62$) are considered to discuss the dynamics of the derived universe. This paper is structured as follows: In section 2, we introduce the basic field equation of the Bianchi-V universe. In Section 3, we discussed the observational constraints of the model parameter. In Section 4, we have discussed the non-interacting and interacting models. The physical behavior of the model is analyzed in Section 5. In Section 6, we apply the Statefinder diagnostic. Conclusions are mentioned in section 7.

2 Field Equations of Bianchi type-V model

The action for Brans-Dicke theory is given by

$$S = \frac{1}{16\pi} \int \sqrt{-g} \left(\phi R - \omega \frac{\phi_{,i}\phi^{,i}}{\phi} \right) d^4x + \frac{1}{16\pi} \int \sqrt{-g} L_m d^4x, \quad (1)$$

where L_m stands for Lagrangian matter field, ϕ denotes the Brans-Dicke scalar field and ω is the Brans-Dicke coupling constant.

The field equations in Brans-Dicke theory [60, 61] by assuming dark matter (DM) and dark energy (DE) are read as:

$$R_{ij} - \frac{1}{2} R g_{ij} = -\frac{8\pi}{\phi} (T_{ij}^m + T_{ij}^{de}) - \frac{\omega}{\phi^2} \left(\phi_i \phi_j - \frac{1}{2} g_{ij} \phi_k \phi^k \right) - \frac{1}{\phi} (\phi_{ij} - g_{ij} \square \phi), \quad (2)$$

and

$$\square\phi = \frac{8\pi}{(3+2\omega)} (T^m + T^{de}), \quad (3)$$

where $T_{ij}^m = \text{dia} [-1, \omega_m, \omega_m, \omega_m] \rho_m$ and $T_{ij}^{de} = \text{dia} [-1, \omega_{de}, \omega_{de}, \omega_{de}] \rho_{de}$ are respectively the energy momentum tensors for DM and DE.

The energy conservation equation is read as

$$(T_{ij}^m + T_{ij}^{de})_{;j} = 0, \quad (4)$$

which leads to

$$\rho_{de} \dot{\omega} + 3H(1 + \rho_m + \omega_{de})\rho_{de} + \dot{\rho}_m = 0 \quad (5)$$

We consider the Bianchi type-V metric of the form

$$ds^2 = dt^2 - A(t)^2 dx^2 - e^{-2\alpha x} [B(t)^2 dy^2 + C(t)^2 dz^2], \quad (6)$$

where α is a constant and the functions $A(t)$, $B(t)$ and $C(t)$ are the three anisotropic directions of expansion in normal three dimensional space. Those three functions are equal in FRW models due to the radial symmetry and so we have only one function $a(t)$ there. The average scale factor a , the spatial volume V and the average Hubble's parameter H are defined as $a = (ABC)^{1/3}$, $V = a^3 = ABC$, and $H = \frac{1}{3} \left(\frac{\dot{A}}{A} + \frac{\dot{B}}{B} + \frac{\dot{C}}{C} \right)$ respectively.

In a comoving coordinate system, the field equations given by Eqs. (2) and (3), for Bianchi type-V spacetime mentioned in Eq. (6) with energy-momentum tensors defined previously, are read as

$$\frac{\ddot{B}}{B} + \frac{\ddot{C}}{C} + \frac{\dot{B}\dot{C}}{BC} - \frac{\alpha^2}{A^2} + \frac{\omega\dot{\phi}^2}{2\phi^2} + \frac{\dot{\phi}}{\phi} \left(\frac{\dot{B}}{B} + \frac{\dot{C}}{C} \right) + \frac{\ddot{\phi}}{\phi} = -\phi^{-1} p_{de} \quad (7)$$

$$\frac{\ddot{C}}{C} + \frac{\ddot{A}}{A} + \frac{\dot{C}\dot{A}}{CA} - \frac{\alpha^2}{A^2} + \frac{\omega\dot{\phi}^2}{2\phi^2} + \frac{\dot{\phi}}{\phi} \left(\frac{\dot{C}}{C} + \frac{\dot{A}}{A} \right) + \frac{\ddot{\phi}}{\phi} = -\phi^{-1} p_{de} \quad (8)$$

$$\frac{\ddot{A}}{A} + \frac{\ddot{B}}{B} + \frac{\dot{A}\dot{B}}{AB} - \frac{\alpha^2}{A^2} + \frac{\omega\dot{\phi}^2}{2\phi^2} + \frac{\dot{\phi}}{\phi} \left(\frac{\dot{A}}{A} + \frac{\dot{B}}{B} \right) + \frac{\ddot{\phi}}{\phi} = -\phi^{-1} p_{de} \quad (9)$$

$$\frac{\dot{A}\dot{B}}{AB} + \frac{\dot{B}\dot{C}}{BC} + \frac{\dot{C}\dot{A}}{CA} - \frac{3\alpha^2}{A^2} - \frac{\omega\dot{\phi}^2}{2\phi^2} + \frac{\dot{\phi}}{\phi} \left(\frac{\dot{A}}{A} + \frac{\dot{B}}{B} + \frac{\dot{C}}{C} \right) = \phi^{-1} (\rho_m + \rho_{de}) \quad (10)$$

$$2\frac{\dot{A}}{A} - \frac{\dot{B}}{B} - \frac{\dot{C}}{C} = 0 \quad (11)$$

$$\frac{\ddot{\phi}}{\phi} + \frac{\dot{\phi}}{\phi} \left(\frac{\dot{A}}{A} + \frac{\dot{B}}{B} + \frac{\dot{C}}{C} \right) = \frac{\rho_{de}(1 - 3\omega_{de}) + \rho_m}{(3 + 2\omega)} \quad (12)$$

From Eqs. (7)- (9), we have

$$\frac{\ddot{A}}{A} + \frac{\dot{A}\dot{C}}{AC} - \left(\frac{\ddot{B}}{B} + \frac{\dot{B}\dot{C}}{BC} \right) + \frac{\dot{\phi}}{\phi} \left(\frac{\dot{A}}{A} - \frac{\dot{B}}{B} \right) = 0 \quad (13)$$

$$\frac{\ddot{B}}{B} - \frac{\ddot{C}}{C} + \frac{\dot{A}\dot{B}}{AB} - \frac{\dot{A}\dot{C}}{AC} + \frac{\dot{\phi}}{\phi} \left(\frac{\dot{B}}{B} - \frac{\dot{C}}{C} \right) = 0 \quad (14)$$

$$\frac{\ddot{C}}{C} - \frac{\ddot{A}}{A} + \frac{\dot{B}\dot{C}}{BC} - \frac{\dot{A}\dot{B}}{AB} + \frac{\dot{\phi}}{\phi} \left(\frac{\dot{C}}{C} - \frac{\dot{A}}{A} \right) = 0 \quad (15)$$

Integrating Eq. (11) and omitting constant of integration, we get

$$\begin{aligned} BC &= A^2 \\ \Rightarrow C &= AD, \text{ \& } B = A/D, \end{aligned} \quad (16)$$

here $D = D(t)$ denotes the measures of anisotropy in the Bianchi-V model.

From Eqs. (14) and (16), we obtain

$$\left(\frac{\ddot{D}}{D} - \frac{\dot{D}^2}{D^2} \right) + \frac{\dot{D}}{D} \left(3\frac{\dot{A}}{A} + \frac{\dot{\phi}}{\phi} \right) = 0, \quad (17)$$

which on integration reduces to

$$D = \exp \left(\int c_1 A^{-3} \phi^{-1} dt \right) \quad (18)$$

where c_1 is the integration constant.

Usng Eq. (16), we can determine the scale factor as $a^3 = A^3 \Rightarrow a = A$.

Thus, we get the following equations finally,

$$2\frac{\ddot{a}}{a} + \frac{\dot{a}^2}{a^2} - \frac{\alpha^2}{a^2} + \frac{c_1^2}{a^6 \phi^2} + \frac{\omega \dot{\phi}^2}{2 \phi^2} + 2\frac{\dot{\phi} \dot{a}}{\phi a} + \frac{\ddot{\phi}}{\phi} = -\phi^{-1} p_{de}, \quad (19)$$

$$3\frac{\dot{a}^2}{a^2} - 3\frac{\alpha^2}{a^2} - \frac{c_1^2}{a^6 \phi^2} - \frac{\omega \dot{\phi}^2}{2 \phi^2} + 3\frac{\dot{\phi} \dot{a}}{\phi a} = \phi^{-1} (\rho_m + \rho_{de}), \quad (20)$$

$$\frac{\ddot{\phi}}{\phi} + 3\frac{\dot{\phi} \dot{a}}{\phi a} = \frac{\rho_{de}(1 - 3\omega_{de}) + \rho_m}{(3 + 2\omega)}. \quad (21)$$

On solving these equation we get dyanamic features of the proposed model.

Authors [62,63] have considered the funtional relation of Brans-Dicke scalar field ϕ and scale factor a as

$$\phi = \phi_0 a^\eta, \quad (22)$$

where η and ϕ_0 are constants. Choice of $\phi = \phi_0 a^\eta$ leads to be consistent with results [64].

The observations of type Ia supernovae [65–67], ‘‘CMB anisotropies’’ [68], and the ‘‘Planck Collaborations’’ [69] have verified that the universe is currently expanding speedly, which was decelerating in past. As a result, the universe must have a ‘‘signature flipping’’ from past

deceleration to current acceleration [70,71]. To determine the explicit solutions of transitioning universe, we have considered a special parameterization of the Hubble parameter $H = \frac{\dot{a}}{a} = \beta(1 + a^{-n})$, where $\beta > 0$, $n > 1$ are constants, first integrate the Hubble parameter and omitted the constant of integration we obtained the scale factor as $a(t) = (e^{n\beta t} - 1)^{\frac{1}{n}}$ [59], which is to be constrained through observations. Now, the Brans–Dicke scalar field ϕ reads as

$$\phi = \phi_0 \left[(e^{n\beta t} - 1)^{\frac{1}{n}} \right]^\eta \quad (23)$$

The deceleration parameter (DP) q is obtained as

$$q = \frac{n}{e^{n\beta t}} - 1 \quad (24)$$

By using the relation $(1 + z) = \frac{a_0}{a}$, we express the cosmological parameters in terms of redshift. Thus, by applying the above transformation, t in terms of z can be found as $\frac{1}{n\beta}(\log(1 + (1 + z)^n))$. To describe the dynamics of the Universe, the Hubble parameter H in terms of redshift can be read as

$$H(z) = \beta[(1 + z)^n + 1]. \quad (25)$$

or

$$H(z) = \frac{H_0}{2}(1 + (1 + z)^n). \quad (26)$$

In order to describe the dynamics properties of the model and the behaviour of physical parameters, we discuss two observational data sets in following section.

3 Observational constraints of the model

3.1 Observational Hubble data set (OHD)

In this section, we have estimate the model parameters n and H_0 using recent 46 points of the $H(z)$ data set (OHD) in the red-shift range $0 \leq z \leq 2.36$ and their corresponding standard deviation σ_i . These 46 OHD points are summarized in the Table-I [61]- [82]. The best fit value of model parameters n and H_0 obtained using χ^2 statistic, which is equivalent to the maximum likelihood analysis given as

$$\chi_{OHD}^2(n, H_0) = \sum_{i=1}^{46} \frac{(H_{th}(n, H_0, z_i) - H_{ob}(z_i))^2}{\sigma(i)^2}, \quad (27)$$

where ‘ H'_{th} and ‘ H'_{obs} denote respectively the theoretical and observed value of Hubble parameter H . By analysis, we found the values of parameters $n = 1.457 \pm 0.042$ and $H_0 = 68.46 \pm 1.97$ $km/s/Mpc$, which are comparable with the current Hubble parameter from Planck 2014 results [84].

Table 1: The OHD data set of Hubble parameter $H(z)$

<i>S.No</i>	<i>Z</i>	<i>H(Obs)</i>	σ_i	References	<i>S.No</i>	<i>Z</i>	<i>H(Obs)</i>	σ_i	References
1	0	67.77	1.30	[74]	24	0.4783	80.9	9	[69]
2	0.07	69	19.6	[75]	25	0.48	97	60	[64]
3	0.09	69	12	[76]	26	0.51	90.4	1.9	[68]
4	0.01	69	12	[64]	27	0.57	96.8	3.4	[78]
5	0.12	68.6	26.2	[75]	28	0.593	104	13	[66]
6	0.17	83	8	[64]	29	0.60	87.9	6.1	[70]
7	0.179	75	4	[66]	30	0.61	97.3	2.1	[68]
8	0.1993	75	5	[66]	31	0.68	92	8	[66]
9	0.2	72.9	29.6	[75]	32	0.73	97.3	7	[61]
10	0.24	79.7	2.7	[77]	33	0.781	105	12	[66]
11	0.27	77	14	[64]	34	0.875	125	17	[66]
12	0.28	88.8	36.6	[75]	35	0.88	90	40	[64]
13	0.35	82.7	8.4	[67]	36	0.9	117	23	[64]
14	0.352	83	14	[66]	37	1.037	154	20	[66]
15	0.38	81.5	1.9	[68]	38	1.3	168	17	[64]
16	0.3802	83	13.5	[69]	39	1.363	160	33.6	[79]
17	0.4	95	17	[76]	40	1.43	177	18	[64]
18	0.4004	77	10.2	[69]	41	1.53	140	14	[64]
19	0.4247	87.1	11.2	[69]	42	1.75	202	40	[64]
20	0.43	86.5	3.7	[77]	43	1.965	186.5	50.4	[79]
21	0.44	82.6	7.8	[70]	44	2.3	224	8	[80]
22	0.44497	92.8	12.9	[69]	45	2.34	222	7	[81]
23	0.47	89	49.6	[71]	46	2.36	226	8	[82]

3.2 Pantheon data

In this part, we fit the Pantheon data (the latest compilation of SNIa with 40 binned in the redshift range $0.014 \leq z \leq 1.62$) to get the best fit values of model parameters n and H_0 , by minimizing $\chi^2(\mu_0, n, H_0)$ statistic:

$$\chi^2(\mu_0, n) = \sum_{i=1} \frac{[\mu_{th}(z(\mu_0, n, z_i)) - \mu_{obs}(z_i)]^2}{\sigma(i)^2} \quad (28)$$

“ μ_{th} and μ_{obs} ” are represents as the theoretical and observed distance modulus. $\sigma(i)$ denotes the standard error of the observed values.

The distance modulus $\mu(z)$ is read by

$$\mu = m - M = \mu_0 + 5 \log_{10} D_L(z), \quad (29)$$

where m and M are “apparent magnitude and absolute magnitude” of any distant luminous object respectively. The parameter μ_0 and the luminosity distance $D_L(z)$ are defined as

$$\mu_0 = 5 \log_{10} \left[\frac{H_0^{-1}}{Mpc} \right] + 25, \quad (30)$$

and

$$D_L(z) = (1+z) \int_0^z \frac{dz}{H(z)}. \quad (31)$$

The absolute magnitude M and apparent magnitude m are read as

$$M = 16.08 - 25 + 5 \log_{10} \left(\frac{H_0}{0.026} \right), \quad (32)$$

$$m = 16.08 + 5 \log_{10} \left(\frac{(1+z)}{0.026} \int_0^z \frac{dz}{H(z)} \right). \quad (33)$$

The best fit contour plots for the $H(z)$ data set and Pantheon data set and their combined data set are shown in this figures 1a, 1b & 1c.

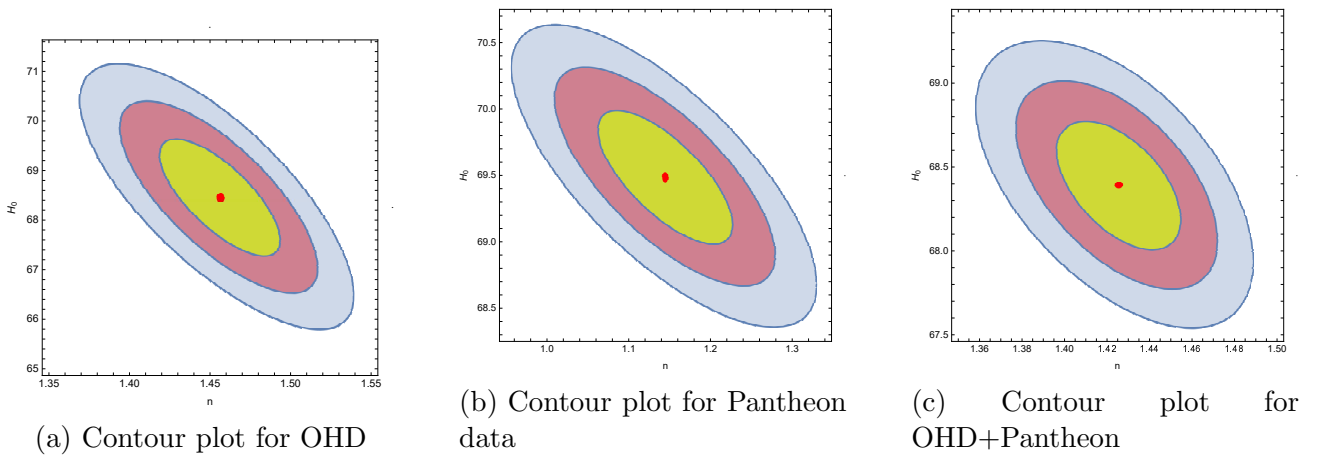


Figure 1: In this figure, the contour plots for likelihood values of model parameters H_0 & n with samples of OHD and Pantheon data and combined datasets are displayed at $1 - \sigma$, $2 - \sigma$, and $3 - \sigma$ levels.

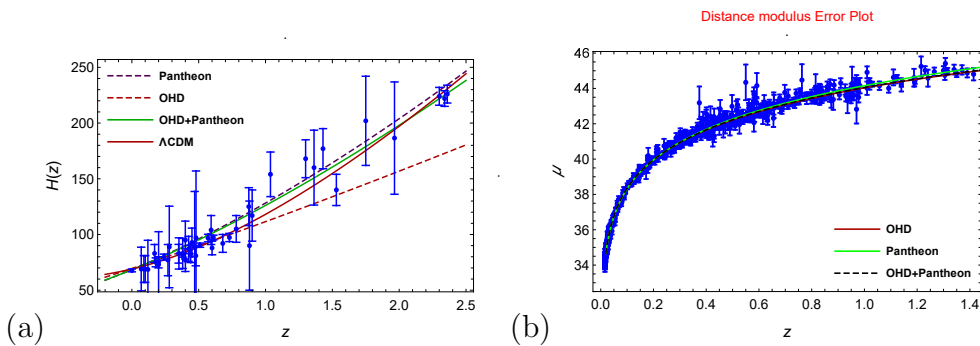


Figure 2: Fig.2a shows the comparison of theoretical model with error bar plots of the OHD data and the Λ CDM model. Table 1 summarises the experimental data in the points with bars. When we perform joint analysis of two datasets, it is evident that our generated model is best-fitted to data. The distance modulus error plot of the Pantheon data and the Λ CDM are shown in Figure 2b, respectively.

Using a differential age technique and galaxy clustering method, many cosmologists [86,87] have computed the values of the Hubble constant at various red-shifts. They described several

observed Hubble constant Hob values as well as corrections in the range $0 \leq z \leq 2.36$ [61,88]. In our derived model the observed and theoretical values are found to agree quite well, indicating that our model is correct. The dots indicate the 46 observed Hubble constant (Hob) values with corrections, while the linear curves show the theoretical Hubble constant $H(z)$ graphs with marginal corrections.

4 Non-Interacting Model

We suppose that DM and DE only interact gravitationally in the non-interacting model, therefore each source must satisfy the continuity equation independently. Thus, from Eq. (4), we have

$$\dot{\rho}_m + 3H\rho_m = 0, \quad (34)$$

$$\dot{\rho}_{de} + 3H\rho_{de}(1 + \omega_{de}) = 0. \quad (35)$$

The energy density of dark matter is calculated by using Eq. (34)

$$\rho_m = \rho_0 a^{-3} = \rho_0 (e^{n\beta t} - 1)^{-\frac{3}{n}} \quad (36)$$

The energy density of dark energy is calculated by using Eqs. (23) and (36) in Eq. (20).

$$\rho_{de} = \phi_0 (e^{\beta nt} - 1)^{\eta/n} \left[-\frac{c_1^2 (e^{\beta nt} - 1)^{-6/n} \left((e^{\beta nt} - 1)^{1/n} \right)^{-2\eta}}{\phi_0^2} - 3\alpha^2 (e^{\beta nt} - 1)^{-2/n} - \frac{\beta^2 (\eta^2 \omega - 6\eta - 6) e^{2\beta nt}}{2(e^{\beta nt} - 1)^2} \right] - \rho_0 (e^{\beta nt} - 1)^{-3/n} \quad (37)$$

Using the values of ϕ and ρ_{de} , the value of EoS parameter is obtained as

$$\omega_{de} = -\frac{\left[\frac{c_1^2 (e^{\beta nt} - 1)^{-6/n} \left((e^{\beta nt} - 1)^{1/n} \right)^{-2\eta}}{\phi_0^2} - \alpha^2 (e^{\beta nt} - 1)^{-2/n} + \frac{\beta^2 e^{\beta nt} \left((\eta^2 (\omega + 2) + 4\eta + 6) e^{\beta nt} - 2(\eta + 2)n \right)}{2(e^{\beta nt} - 1)^2} \right]}{\left[-\frac{c_1^2 (e^{\beta nt} - 1)^{-6/n} \left((e^{\beta nt} - 1)^{1/n} \right)^{-2\eta}}{\phi_0^2} - 3\alpha^2 (e^{\beta nt} - 1)^{-2/n} - \frac{\beta^2 (\eta^2 \omega - 6\eta - 6) e^{2\beta nt}}{2(e^{\beta nt} - 1)^2} \right] - \frac{\rho_0}{\phi_0} (e^{\beta nt} - 1)^{-(3+\eta)/n}}. \quad (38)$$

5 Interacting Model

We discuss the interacting cosmological models of the universe by considering the interaction between DE and DM components. As a result, the DM and DE the continuity equations are written as

$$3H\rho_m + \dot{\rho}_m - Q = 0, \quad (39)$$

$$3H\rho_{de}(1 + \omega_{de}) + \dot{\rho}_{de} + Q = 0. \quad (40)$$

The coupling between DM and DE is denoted by Q . We estimate the coupling between DE and DM as a function of ρ_m and H , $Q \propto \rho_m H$. As a result, for the interaction model, we use

“ $Q = 3b^2\rho_m H$ ”; b^2 is a constant.

Now, the energy densities of DM and DE are determined as follows:

$$\rho_m = k (e^{\beta nt} - 1)^{\frac{3(b^2-1)}{n}}. \quad (41)$$

Here, k is an integration constant.

$$\rho_{de} = \phi_0 (e^{\beta nt} - 1)^{\eta/n} \left[-\frac{c_1^2 (e^{\beta nt} - 1)^{-6/n} \left((e^{\beta nt} - 1)^{1/n} \right)^{-2\eta}}{\phi_0^2} - 3\alpha^2 (e^{\beta nt} - 1)^{-2/n} - \frac{\beta^2 (\eta^2 \omega - 6\eta - 6) e^{2\beta nt}}{2(e^{\beta nt} - 1)^2} \right] - k (e^{\beta nt} - 1)^{\frac{3(b^2-1)}{n}} \quad (42)$$

For interacting model, the EoS parameter is obtained as:

$$\omega_{de} = -\frac{\left[\frac{c_1^2 (e^{\beta nt} - 1)^{-6/n} \left((e^{\beta nt} - 1)^{1/n} \right)^{-2\eta}}{\phi_0^2} - \alpha^2 (e^{\beta nt} - 1)^{-2/n} + \frac{\beta^2 e^{\beta nt} \left((\eta(\eta(\omega+2)+4)+6) e^{\beta nt} - 2(\eta+2)n \right)}{2(e^{\beta nt} - 1)^2} \right]}{\left[-\frac{c_1^2 (e^{\beta nt} - 1)^{-6/n} \left((e^{\beta nt} - 1)^{1/n} \right)^{-2\eta}}{\phi_0^2} - 3\alpha^2 (e^{\beta nt} - 1)^{-2/n} - \frac{\beta^2 (\eta(\eta\omega - 6) - 6) e^{2\beta nt}}{2(e^{\beta nt} - 1)^2} \right] - \frac{k}{\phi_0} (e^{\beta nt} - 1)^{\frac{3(b^2-1-\eta)}{n}}} \quad (43)$$

6 Physical properties and dynamical behaviour of model

The evolution of density parameter for DM and DE are shown in Fig. 3

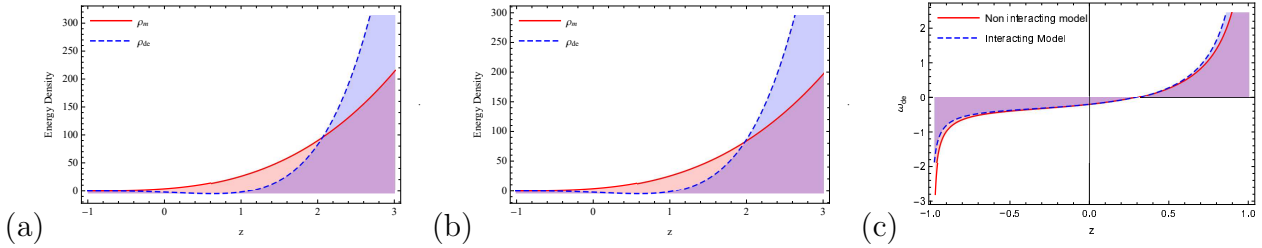


Figure 3: Plots of DM and DE energy densities versus redshift z for non-interacting (left) and interacting (right) models & EoS parameter

Figure 3(a) shows the energy density for dark matter for the interacting and non-interacting cases with respect to redshift. Figure 3(b) shows the variation of energy density for DE versus redshift. In both figures, we conclude that as $\rho \rightarrow 0$ for (or $z \rightarrow -1$) which is consistent with a well-established scenario. From figure 3c, it is clear that the EoS of DE is varying in quintessence region and crossing the Phantom Divide line (PDL) $\omega_{de} = -1$ and finally enters in the phantom region in both interacting and non-interacting cases. The curve exhibits a negative tendency before evolving through several stages of acceleration, deceleration, and finally reaching to phantom phase.

The possibility of universe evolution is indicated by the shift from one phase to the next.

6.1 Age of universe

The age of the universe is obtained as

$$dt = -\frac{dz}{(1+z)H(z)} \implies \int_t^{t_0} dt = -\int_z^0 \frac{1}{(1+z)H(z)} dz. \quad (44)$$

Using Eq. (26), we get

$$t_0 - t = \int_0^z \frac{2}{H_0(z+1)[(z+1)^n + 1]} dz, \quad (45)$$

where t_0 is the ‘‘present age of universe’’ and it is given by

$$t_0 = \lim_{x \rightarrow \infty} \int_0^x \frac{2}{H_0(z+1)[(z+1)^n + 1]} dz. \quad (46)$$

Integrating Eq.(43), we get

$$H_0 t_0 = 0.9425 \quad (47)$$

In this study, we have calculated the numerical value of H_0 as $0.07173 \text{ Gyr}^{-1} \sim 70.29 \text{ kms}^{-1} \text{ Mpc}^{-1}$. Therefore, the present age of the universe for the derived model is obtained as $t_0 = \frac{0.9425}{H_0} = 13.14$ Gyrs. Figure 7 shows the variation of ‘‘ $H_0(t_0 - t)$ ’’ with redshift z . According to WMAP data [55], the empirical value of current age of the universe is $t_0 = 13.73_{-0.17}^{+0.13}$. It’s worth noting that $t_0 = 13.81 \pm 0.038$ Gyrs is the current age of the universe in Planck collaboration results [89]. The universe’s present has been calculated as 14.46 ± 0.8 Gyrs [104], 14.3 ± 0.6 Gyrs [105] and 14.5 ± 1.5 Gyrs [106] in various cosmological studies.

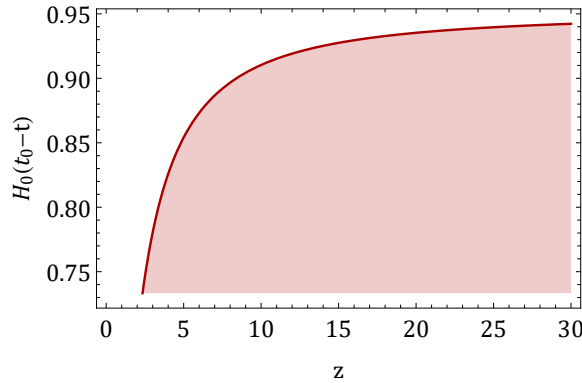


Figure 4: The plot of $H_0(t_0 - t)$ versus z

6.2 Deceleration parameter

Figure 5 depicts the dynamics of the decelerating parameter (q) with respect to z . The models for OHD and (OHD+Pantheon) coincide with Λ CDM with the signature flipping at $z_t = 0.809$ while for Pantheon data model shows signature flipping at $z_t = 4.44123$ due to the dominance of DE in the universe. As a result, the current universe evolves with a negative sign of q , causing the accelerated expansion of the universe. Moreover the reconstruction of $q(z)$ is done by the joined ($SNIa + CC + H_0$), which have obtained the transition redshift $z_t = 0.69_{-0.06}^{+0.09}$, $0.65_{-0.07}^{+0.10}$ and $0.61_{-0.08}^{+0.12}$ within (1σ) [90]. which are seen as well consistent with past outcomes [91–95]

including the Λ CDM expectation $z_t \approx 0.7$. $0.6 \leq z_t \leq 1.18$ (2σ , joint examination) [96] is the other limit of transition redshift.

The recent 36 observational Hubble data (OHD) provides the redshift range $0.07 \leq z \leq 2.36$ [97]. The joint light curves (JLA) sample, comprised of 740 type-Ia supernovae (SN Ia) indicates the redshift range $0.01 \leq z \leq 1.30$. In this way, our developed model depicts a transition from the early deceleration phase to the current speeding phase for OHD, Pantheon, (OHD+Pantheon) data. Furthermore, we find that the deceleration parameter will remain negative in the future, $z \rightarrow -1$, $q \rightarrow -1$.

The DP in terms of the redshift z can be written as

$$q(z) = \frac{(n-1)(1+z)^n - 1}{1 + (1+z)^n} \quad (48)$$

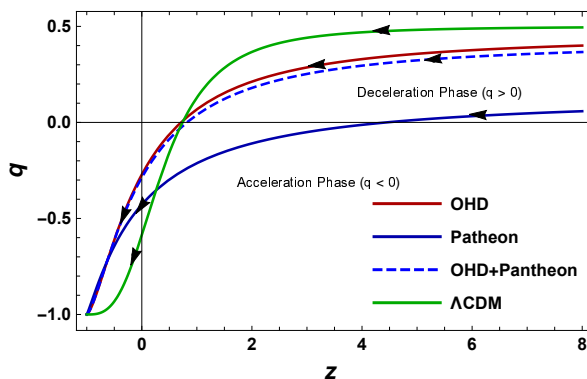


Figure 5: Plot of deceleration parameter q versus z .

6.3 Luminosity Distance

The redshift-luminosity distance connection [98] is a significant observational tool for studying the universe's evolution. The luminosity distance (D_L) is calculated in terms of the redshift, which occurs when light coming out of a distant luminous body is redshifted due to the expansion of the cosmos. The luminosity distance is used to calculate a source's flux. It's written as $D_L = a_0 r(1+z)$, where r denotes the radial coordinate of the source. For the model, the radial coordinate r is obtained as $r = \int_0^{dr} = \int_0^t \frac{cdt}{a(t)} = \frac{1}{a_0 H_0} \int_0^z \frac{cdz}{h(z)}$, where $h(z) = \frac{H(z)}{H_0}$.

Therefore, we get the luminosity distance as

$$\frac{H_0 D_L}{c} = (1+z) \int_0^0 \frac{dz}{h(z)} \quad (49)$$

6.4 Particle horizon

The particle horizon is a measurement of the size of the observable cosmos [99]. The particle horizon is reads as

$$R_P = \lim_{t_P \rightarrow 0} a_0 \int_{t_0}^{t_P} \frac{dt}{a(t)} = \lim_{z \rightarrow \infty} \int_0^z \frac{dz}{H(z)} \quad (50)$$

where t_p denotes the "time in past" at which the light signal is sent from the source. When we integrate Eq. (29) for a large value of red-shift, we get $R_P = 2.7845 H_0^{-1}$ as the particle horizon. Figure 6 depicts the dynamics of correct distance vs red-shift. We can see from Figure 7 that when $z = 0$, $a_0 H_0 x$ is null, implying that when $z = 0$, the appropriate distance x becomes infinite. Thus we are at very large distance (\sim at infinite distance) from an event occurred in the beginning of the universe.

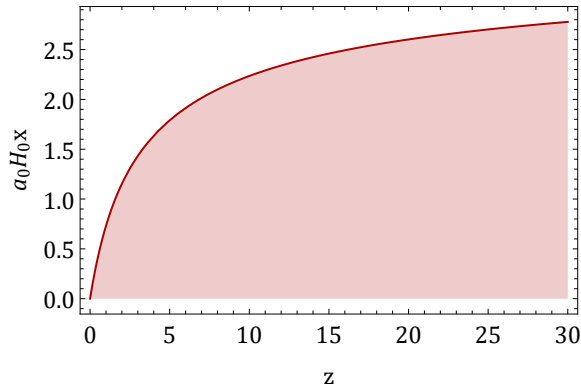


Figure 6: Distance of particle horizon versus z

7 Statefinder diagnostics

The statefinder pairs $\{r, s\}$ are the geometrical quantities that are directly obtained from the metric. This diagnostic is used to distinguish different dark energy models and hence becomes an important tool in modern cosmology. The statefinder parameters r and s have been defined as follows [100–102]

$$r = \frac{\ddot{a}}{aH^3}, \quad s = \frac{r - 1}{3(q - \frac{1}{2})} \quad (51)$$

$$r = \frac{n^2 (2(z+1)^n + 1) (z+1)^n}{((z+1)^n + 1)^2} - \frac{3n(z+1)^n}{(z+1)^n + 1} + 1 \quad (52)$$

$$s = \frac{2n(z+1)^n (2n(z+1)^n - 3((z+1)^n + 1) + n)}{3((z+1)^n + 1) (2n(z+1)^n - 3((z+1)^n + 1))} \quad (53)$$

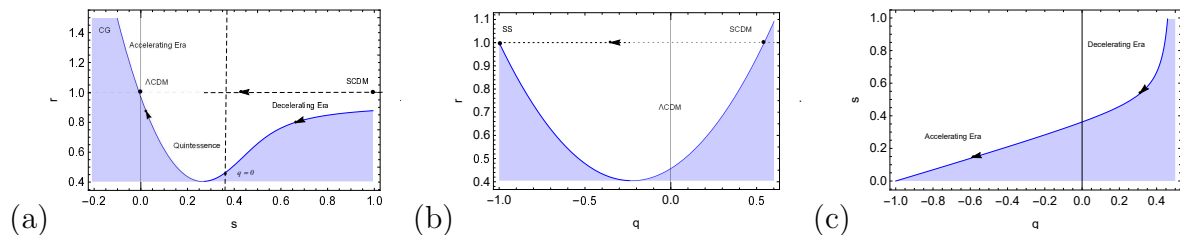


Figure 7: Plots of statefinders $(r - s)$ $(r - q)$ and $(s - q)$ versus redshift z .

The statefinder diagnostic is a valuable tool in current cosmology used to differentiate various dark energy models [100–103]. Different trajectories in the $(r - s)$ $(r - q)$ and $(s - q)$ planes

express the time evolution for various dark energy models. The present model initially lies in quintessence region ($r < 1, s > 0$), passes through the Λ CDM (r, s) = (1, 0) and finally approaches to Chaplygin gas region $r > 1$ and $s < 0$ as clearly seen in Fig.7a. The statefinder pair for Λ CDM and standard cold dark matter(SCDM) are respectively (r, s) = (1, 0) and (r, s) = (1, 1) depicts in the framework of Bianchi-V background. To get more information on the parametrization, we analyzed the temporal growth of our model by the ($r - q$) plane. In Fig. 7(b) The solid line in the diagnostic plane's shows the evolution of the Λ CDM cosmological model. Initially our model start with the SCDM point (r, q) = (1, -0.5) passing the Λ CDM (r, q) = (1, 0) point and finally reaches to SS point (r, q) = (1, -1). The SCDM universe is clearly represented by the $q > 0$ and $r > 1$ area of the profile. The $s - q$ trajectory begins with a decelerating period and progress to an accelerating era (see Fig.7c).

Table 2: Constrained values of the model parameters with minimum χ^2 values

Datasets	n	H_0	$q(z = 0)$	z_t	χ^2
$H(z)$	1.457 ± 0.042	68.46 ± 1.97	-0.2715	0.711645	31.8169
Pantheon	1.144 ± 0.085	69 ± 0.49	-0.428	4.44123	569.787
$H(z)$ +Pantheon	1.426 ± 0.030	68.39 ± 0.40	-0.287	0.8192	628.552

8 Conclusion

In this paper, first, we observed the cosmological parameters for the observable universe in Bianchi type V space time in Branc Dicke theory. Second, we used statistical χ^2 tests to limit the various model parameters of the universe in the resultant model. Table-2 summaries the major findings of the statistical analysis.

The main objective of this article is to use independent observables such as Pantheon dataset, OHD, and their joint combination (OHD+Pantheon) to constrain the free parameters of the theoretical models, which potentially increase the sensitivity of our estimations. Out of these measurements, we specifically discuss the H_0 determination. The main features of the derived model are discussed in the following manner:

- First, we have found a perfect solution to Einstein's field equations for both interacting and non-interacting cases in Bianchi type V space-time.
- We have calculated best-fitted values of the model parameters from the marginal 1σ , 2σ , and 3σ contour plots of OHD, Pantheon, and (OHD+Pantheon) as shown in Fig.1. The constraints on H_0 and n for the derived model by fitting the OHD points and the estimate of Hubble's constant agree closely with Riess et al. [1].
- In Fig. 2a, we have shown the error bar plots for OHD data set, theoretical model plot for OHD data, and the Λ CDM model. The points with bars indicate the experimental data summarized in Table-1. The 46 points of the $H(z)$ and Union 2.1 compilation data are used to constrain the model parameter n and H_0 . The derived model agrees well with $H(z)$ and Pantheon data and closely resembles the behavior of the Λ CDM. The distance modulus error plot of the Pantheon data alongwith the Λ CDM are shown in Figure 2b.

- Figures 3a and 3b show the graphical behavior of the energy densities for DM and DE. We noticed that ρ_m and ρ_d of the model under discussion are positive decreases with time and vary individually with redshift in both interacting and non-interacting scenarios. Figure 3c shows the variation of the DE (ω_{de}) equation of state parameter versus redshift for interacting and non-interacting models.

It has been observed that (ω_{de}) begins in the positive and ends in the negative. Note that $\omega_{de} > -1$ and $\omega_{de} < -1$ respectively indicate quintessence and phantom regimes. While $\omega_{de} = -1$ represents a universe dominated by cosmological constant. This nature of EoS is ruled out by SN Ia findings. As a result, the evolving range of ω_{de} of our derived model favors the phantom universe in the present epoch.

- The age of the universe in the derived model is 13.14 Gyrs, as determined by OHD observations (see Fig. 4). The current age of the universe is believed to be $t_0 = 13 : 65$ Gyrs. This age of the cosmos is very similar to the results found through Plank's observation [89] and several other observations [104–106].
- In our derived model, there is a smooth transition from decelerating to accelerating phase, which is consistent with the present scenario of the modern cosmology (see Fig. 5). We have plotted the deceleration parameter q by getting its numerical solution, which exhibits a transition at $z_t = 0.711$, from the early decelerated phase to a late time accelerated phase. This is in good agreement with the current cosmological observations. We have depicted that the deceleration parameter for OHD, (OHD+Pantheon) coincide with the Λ CDM model and have the same transition point(see Fig. 5).
- Particle horizon exists in the derived model, and its value differs from the Λ CDM universe model (see Fig.6). The age of the universe in the developed model matches the empirical value obtained from WMAP measurements and Plank collaborations quite well.
- The variation of the trajectories $r - s$, $r - q$ and $s - q$ planes are depicted in Fig. 7. In the diagram, the paths of the $r - s$ trajectories are depicted by arrows, which represent various dark energy models, and eventually approach to Λ CDM (see Fig. 7a). The evolution of the trajectories begins at SCDM in the $r - q$ plane diagram, and as time passes, the trajectories of the $r - q$ approach the steady-state model SS (see Fig. 7b). The $s - q$ trajectories begin with a decelerating period and progress to an accelerating era (see Fig. 7c).

We noticed the range of the deceleration parameter from the equation of $q(z)$, which clearly demonstrates the signature flipping behavior. As a result, we find that the current OHD and Pantheon data give well-constrained H_0 values, and our model is consistent with recent observations. Furthermore, we describe the dynamics of the cosmos for both interacting and non-interacting scenarios.

Acknowledgments

A. Pradhan is thankful to IUCAA, Pune, India for providing support and facility under Visting Associateship prpgram.

References

- [1] A.G. Riess et al., *Astron. J.* **116**, 1009 (1998).
- [2] S. Perlmutter et al., *Astrophys. J.* **517**, 565 (1999).
- [3] S. Capozziello, *Phys. Lett. B* **639**, 135 (2006).
- [4] S. Carroll, *Phys. Rev. D* **70**, 043528 (2004).
- [5] K. Bamba et al., *Astrophys. Space Sci.* **342**, 155 (2012).
- [6] S. Nojiri, S.D. Odintsov, *Phys. Rep.* **505**, 2 (2011)
- [7] M. F. Shamir, *Exp. Theor. Phys*, **123**, 607 (2016).
- [8] A. Pradhan, D. C. Maurya, A. Dixit, *Int. J. Geom. Method Mod. Phys.* **18** 2150124 (2021).
- [9] A. Banerjee, et al., *Europ. Phys. Jour. C* **81**, 10131 (2021).
- [10] A. Pradhan, A. Dixit, *Int. J. Geom. Method Mod. Phys.* **18** 2150159 (2021).
- [11] S. K. Maurya et al., *Mod. Phys. Lett. A* **36** 2150231 (2021).
- [12] T. Tangphati et al., *Mod. Phys. Lett. B* **819** 136423 (2021).
- [13] T. Tangphati et al., *Phys. Dark Univ.* **33** 100877 (2021).
- [14] S. K. Maurya et al., *Europ. Phys. J. C* **81** 848 (2021).
- [15] G. Panotopoulos et al., *Chin. J. Phys.* <http://doi.org/10.1016/j.cjph.2022.01.008> (2022).
- [16] T. Harko et al., *Phys. Rev. D* **84**, 024020 (2011).
- [17] B. M. Barker, *Astrophys. J.* **219**, 5 (1978).
- [18] J. D. Bekenstein, *Phys. Rev. D* **70**, 083509 (2004).
- [19] H. Weyl, *Sitzungsber. Preuss. Akad. Wiss, Berlin* 465 (1918).
- [20] G. Lyra, *Mathematische Zeitschrift* **54**, 52 (1951).
- [21] H. Yilmaz, *Phys. Rev.* **111**, 1417 (1958).
- [22] C. Brans, R.H. Dicke, *Phys. Rev.* **124**, 925 (1961).
- [23] A. Pradhan et al., *Int. J. Geom. Meth. Modern Phys.* **16**, 1950185 (1019).
- [24] C. Aktas et al., *Phys Lett. B* **707**, 237 (2012).
- [25] J. L. Alonso, J. L. Cortes, V. Laliena, *Phys. Rev. D* **67**, 024023 (2003).
- [26] A. Guth, *Phys. Rev. D* **23**, 347 (1981).
- [27] C. Mathiazhagan, V.B. Johri, *Class. Quantum Gravity* **1**, L29 (1984).

- [28] D. La, P.J. Steinhardt, Phys. Rev. Lett. **62**, 376 (1989).
- [29] N. Banerjee, D. Pavon, Phys. Rev. D **63**, 043504 (2001).
- [30] T. Singh, L. N. Rai, Astrophys. Space Sci. **96**, 95 (1983).
- [31] C. Romero, A. Barros, Astrophys. Space Sci. **192**, 263 (1992).
- [32] K. Uehara and C. W. Kim, Phys. Rev. D **26**, 2575 (1982).
- [33] J. M. Servero, P. G. Estevez, Gen. Rel. Grav. **15**, 351 (1983).
- [34] D. Lorenz-Petzold, Phys. Rev. D **29**, 2399 (1984).
- [35] L.O. Pimentel, Astrophys. Space Sci. **112**, 175 (1985).
- [36] T. Etoh, M. Hashimoto, K. Arai, S. Fujimoto, Astron. Astrophys. **325**, 893 (1997).
- [37] H. Amirhashchi, A.K. Yadav, Phys. Dark Univ. **30**, 100711 (2020).
- [38] S. Das, N. Banerjee, Phys. Rev. D **78**, 043512 (2008).
- [39] U. K. Sharma, G. K. Goswami, A. Pradhan, Grav. & Cosmol. **24**, 191 (191).
- [40] A. Chand, R. K. Mishra, A. Pradhan, Astrophys. Space Sci. **361**, 81 (1985).
- [41] T. Singh, T. Singh, J. Math Phys. **25**, 9 (1984).
- [42] A. K. Azad, J. N. Islam, Pramana **60**, 2127 (2003).
- [43] O. Akarsu, et al., Europ. Phys. Jour. C **80**, 1 (2020).
- [44] P. Mukherjee, S. Chakrabarty, Europ. Phys. Jour. C **79**, 681 (2019).
- [45] D. C. Maurya, R. Zia, A. Pradhan, J. Experim. Theor. Phys. **123**, 617 (2016).
- [46] V. K. Bhardwaj, M. K. Rana, A. K. Yadav, Astrophys. Space Sci. **364**, 1 (2019).
- [47] V. K. Bhardwaj, A. K. Yadav, Int. J. Geom. Methods Mod. Phys. **17(10)**, 2050159 (2020).
- [48] V. K. Bhardwaj, Mod. Phys. Lett. A **33** 1850234 (2018).
- [49] N. Ahmed, A. Pradhan, Int. J. Theor. Phys. **53**, 289 (2014).
- [50] H. Amirhashchi, Phys. Rev. D **96**, 123507 (2017).
- [51] A. Pradhan, K. Jotania, Int. J. Theor. Phys. **49**, 1719 (2010).
- [52] A. Pradhan, H. Amirhashchi, Mod. Phys. Lett. A **26**, 2261 (2011).
- [53] A. Pradhan, A. K. Singh, D. S. Chauhan, Int. J. Theor. Phys. **52**, 266 (2013).
- [54] C. P. Singh, Braz. J. Phys. **39**, 619 (2009).
- [55] G. Hinshaw et al., Astrophys. J. Suppl. **288**, 170 (2007).

- [56] G. Hinshaw et al., *Astrophys. J. Suppl.* **180**, 225 (2009).
- [57] A. A. Costa et al., *J. Cosmol. Astropart. Phys.* **01**, 028 (2017).
- [58] R. Adam et al., *Astron. Astrophys.* **594**, A1 (2016).
- [59] R. Nagpal et al., *Eur. Phys. J. C* **78**, 946 (2018).
- [60] A. Pradhan et al., *Int. J. Geom. Methods Mod. Phys.* **16**, 1950185 (2019).
- [61] A. K. Yadav et al., *Phys. Dark Universe* **31**, 100738 (2021).
- [62] A. Sheykhi, *Phys. Lett. B* **681**, 205 (2009).
- [63] V.B. Johari, K. Desikan, *Gen. Relativ. Gravit.* **26**, 1217 (1994).
- [64] D. Stern et al., *J. Cosmol. Astropart. Phys.* **1002**, 008 (2010).
- [65] R. Prasad et al., *Int. J. of Mod. Phys. A* **36**, 2150044 (2021).
- [66] M. Moresco et al., *J. Cosmol. Astropart. Phys.* **08**, 006(2012).
- [67] D. H. Chuang, Y. Wang, *Mon. Not. R. Astro. Soc.* **435**, 255 (2013).
- [68] S. Alam S. et al., *Mon. Not. R. Astro. Soc.* **470**, 2617 (2016).
- [69] M. Moresco et al., *J. Cosmol. Astropart. Phys.* **05**, 014 (2016).
- [70] C. Blake et al., *Mon. Not. R. Astro. Soc.* **425**, 405 (2012).
- [71] A. L. Ratsimbazafy et al., *Mon. Not. R. Astro. Soc.* **467**, 3239 (2017).
- [72] J. P. Singh, *Astrophys. Space Sci.* **318**, 103 (2008).
- [73] N. Banerjee, S. Das, *Gen. Relat. Gravit.* **37**, 1695 (2005).
- [74] E. Macaulay et al., *Mon. Not. R. Astro. Soc.* **486**, 2184 (2019).
- [75] C. Zhang et al., *Res. Astron. Astrophys.* **14**, 1221 (2014).
- [76] J. Simon, L. Verde, R. Jimenez, *Phys. Rev. D* **71**, 123001 (2005).
- [77] E. Gazta Naga et al., *Mon. Not. R. Astro. Soc.* **399**, 1663 (2009).
- [78] L. Anderson et al., *Mon. Not. R. Astro. Soc.* **441**, 24 (2014).
- [79] M. Moresco, *Mon. Not. R. Astro. Soc.* **450**, L16 (2015).
- [80] N. G. Busa et al., *Astron. Astrophys.* **552**, A96 (2013).
- [81] T. Delubac et al., *Astron. Astrophys.* **574**, A59 (2015).
- [82] A. Font-Ribera, et al., *J. Cosmol. Astropart. Phys.* **2014**, 027 (2014).
- [83] P. J. Steinhardt, L. M. Wang, I. Zlatev, *Phys. Rev. D* **59**, 123504 (1999).

- [84] P.A.R. Ade et al., [Planck Collaboration], *Astro. Astrophys.* **571**, A16 (2014).
- [85] N. Suzuki et al., *Astrophys. J.* **746**, 85 (2012)
- [86] L. K. Sharma, A. K. Yadav, P. K. Sahoo, B. K. Singh, *Results Phys.* **10**, 738 (2018).
- [87] Y. Chen, S. Kumar, B. Ratra, *Astrophys. J.* **835**, 86 (2017).
- [88] G. K. Goswami, A. Pradhan, A. Beesham, *Pramana* **93**, 1 (2019).
- [89] N. Aghanim et al., *Astronomy & Astrophysics*, **641** A6 (2020).
- [90] A. A. Mamon, *Mod. Phys. Lett. A* **33**, 1850056 (2018).
- [91] R. Nair et al., *J. Cosmol. Astropart. Phys.* **01**, 018 (2012).
- [92] A. A. Mamon, S. Das, *Int. J. Mod. Phys. D* **25**, 1650032 (2016).
- [93] O. Farooq, B. Ratra, *Astrophys. J.* **766**, L7 (2013).
- [94] J. Magana et al., *J. Cosmol. Astropart. Phys.* **10**, 017 (2014).
- [95] A. A. Mamon, K. Bamba and S. Das, *Eur. Phys. J. C* **77**, 29 (2017).
- [96] J. A. S. Lima et al., arXiv: 1205.4688v3[astro-ph.CO] (2012).
- [97] H. Yu, B. Ratra and Fa-Yin Wang, *Astrophys. J.* **856**, 3 (2018).
- [98] A. R. Liddle, D. H. Lyth, *Phys. Rep.* **231**, 1 (1993).
- [99] B. Margalef-Bentabol et al., *J. Cosmol. Astropart. Phys.* **2013**, 015 (2013).
- [100] S. K. J. Pacif, S. Arora, P. K. Sahoo, *Phys. Dark Universe* **32**, 100804 (2021).
- [101] V. Sahni, T. D. Saini, A. A. Starobinsky and U. Alam, *JETP Lett.* **77**, 201 (2003).
- [102] U. Alam et al., *Mon. Not. R. Astron. Soc.* **344**, 1057 (2003).
- [103] M. Sami et al., *Phys. Rev. D* **86**, 103532 (2012).
- [104] H.E. Bond, E.P. Nelan, D.A. VandenBerg, G.H. Schaefer, D. Harmer, *Astrophys. J.* **765**, L12 (2013).
- [105] S. Masi, et al., *Prog. Part. Nucl. Phys.* **48**, 243 (2002).
- [106] A. Renzini, A. Bragaglia, F.R. Ferraro, *Astrophys. J.* **465**, L23 (1996).